Journal of Applied Polymer Science

Thin film composite forward osmosis membranes with poly(2-hydroxyethyl methacrylate) grafted nano-TiO_2 as additive in substrate

Wu Kuang,[1,2] Zhongnan Liu,[1,2] Guodong Kang,[1] Dandan Liu,[1] Meiqing Zhou,[1] Yiming Cao[1]

[1]Dalian National Library for Clean Energy (DNL), Dalian Institute of Chemical Physics, Chinese Academy of Sciences, Dalian 116023, China

[2]University of Chinese Academy of Sciences, Beijing 100049, China

Correspondence to: Y. Cao (E-mail: ymcao@dicp.ac.cn)

ABSTRACT: The poly(2-hydroxyethyl methacrylate) grafted titanium dioxide nanoparticles were synthesized and added to the substrate of flat-sheet thin film composite forward osmosis (TFC-FO) membranes. The hydrophilicity of substrate was improved, which was advantageous to enhance the water flux of TFC-FO membranes. The membranes containing a 3 wt % TiO_2-PHEMA in the substrate exhibited a finger-like structure combined with sponge-like structure, while those with lower or without TiO_2-PHEMA content showed fully finger-like structures. As for FO performance, the TFC-FO membranes with 3 wt % TiO_2-PHEMA content achieved the highest water flux of 42.8 LMH and 24.2 LMH against the DI water using 2*M* NaCl as the draw solution tested under the active layer against draw solution (AL-DS) mode and active layer against feed solution (AL-FS) mode, respectively. It was proven that the hydrophilic property of membrane substrates was a strong factor influencing the water flux in FO tests. Furthermore, the structural parameter was remarkably decreased with an increase of TiO_2-PHEMA content in membrane substrate, indicating the reducing of internal concentration polarization. © 2016 Wiley Periodicals, Inc. J. Appl. Polym. Sci. **2016**, *133*, 43719.

KEYWORDS: grafting; membranes; nanoparticles; nanowires and nanocrystals; separation techniques

Received 18 January 2016; accepted 1 April 2016

DOI: 10.1002/app.43719

INTRODUCTION

Water crisis is becoming a severe restriction for economy and society development. To resolve the problem, membrane science and technology shows great advantage in water treatment. And among different membrane technologies, forward osmosis (FO) is a promising technology for water purification and seawater/brackish desalination.[1,2] Compared to other pressure-driven membrane processes, such as nanofiltration (NF) and reverse osmosis (RO), FO process utilizes the osmotic pressure difference between the feed and draw solution across a semipermeable membrane as the driving force to persuade the pure water to flow through the membrane from the feed to the draw solution.[3] The osmotic pressures provided in FO can be significantly higher than hydraulic pressures used in RO as the driving force, subsequently resulting in a higher theoretical water flux.[4,5] Moreover, FO also offers the advantages of high rejections to a wide range of contaminants and lower membrane-fouling propensities compared to traditional pressure-driven membrane processes.[6–8]

FO membranes and process have made great progress in the last decade. Thin film composite (TFC) membrane was considered to be the most efficient method for FO membrane preparation because TFC membranes offer the possibility to optimize membrane substrates and selective layers separately.[9,10] In order to reduce internal concentration polarization (ICP), an ideal TFC membrane for FO should consist of a highly porous, highly hydrophilic, and low tortuosity substrate and a highly selective active layer to improve salt rejection and minimize reverse solute diffusion.[11] On the other hand, researchers found that increasing the membrane hydrophilicity is also an effective method to improve pure water flux, as it promotes the wetting of all available pores and reduce structural parameter.[12–19] Physical blending is the mostly used method because of its simplicity and mild modification conditions. Adding hydrophilic additives such as polyvinylpyrrolidone (PVP) and polyethylene glycol (PEG) into the casting solution is a very common method.[13] However, during a long time operation, these additives gradually leached out from membranes, which could lead to membrane instability. Besides the hydrophilic additives, hydrophilic polymers are also used to improve membrane hydrophilicity. Wang *et al.* recently developed substrates for TFC-FO membrane from blend polysulfone (PSf) and sulfonated polysulfone (SPSf) to increase the hydrophilicity

of the PSf substrates. The fabricated flat-sheet membranes show water fluxes up to 47.5 LMH in the AL-DS mode using 2*M* NaCl as the draw solution.[14]

Among those hydrophilic materials, nanomaterials play a significant role in environmental applications particularly to revolutionize century-old conventional water treatment processes due to the great progress in nanotechnology.[20,21] Among all kinds of nanoparticles, TiO_2 has obtained much attention because of its availability, stability, and promise for applications such as catalysis and photocatalysis, battery, membrane, etc.[18,22–24] However, TiO_2 nanoparticles often form agglomerates due to its large surface area. Moreover, the bad compatibility between inorganic nanoparticles and polymers would result in defects in membranes. To resolve those problems, great efforts had been made by different research groups.[25,26] Similarly, Zhu *et al.* modified SiO_2 nanoparticles by grafting poly(2-hydroxyethyl methacrylate) (PHEMA) onto it, and then dispersed into the casting solution. The resultant membrane showed not only superior permeate performance but also anti-fouling or antibacterial property than those without SiO_2 nanoparticles.[26]

Inspired by those research results, in this article, the TiO_2 nanoparticles were modified and used as additive to improve the substrates hydrophilicity to reduce ICP. In this approach, TiO_2 nanoparticles were initially treated with 3-(trimethoxysilyl) propylmethacrylate (MPS); then, PHEMA was grafted onto the surface by radical polymerization method. HEMA has abundant hydrophilic polymer chains and hydroxyl groups which could increase both the particle dispersibility and the hydrophilicity of the composite membrane. By the blending of TiO_2-*g*-PHEMA nanoparticles in PSf substrate, the hydrophilicity of substrate was enhanced. Consequently, a significant improvement in FO membrane performance was achieved with great decrease in membrane structural parameter, indicating the reducing of ICP.

EXPERIMENTAL

Materials

PSf (Udel-3500, Amoco, Alpharetta, Georgia) was dried at 110 °C for 12 h prior to use. TiO_2 nanoparticles (anatase, mean pore size 25 nm, Shanghai, China) and trimesoyl chloride (TMC) were purchased from Aladdin Industrial Corporation. MPS, HEMA, *m*-phenylenediamine (MPD) and 2,2-azobis(isobutyronitrile) (AIBN) were purchased from J&K Scientific Ltd, Beijing, China. Dimethylacetamide (DMAc), *N*-methyl-2-pyrrolidone (NMP), *n*-hexane, polyethylene glycol (PEG-400), absolute ethanol, and sodium chloride (NaCl) were purchased from Tianjin Kemiou Chemical Reagent Co., Ltd, Tianjin, China. DI water was supplied by Kena Science Technology Development Co., Ltd, Dalian, China.

Surface Modification of TiO_2 Nanoparticles

The surface modification of TiO_2 nanoparticles was conducted in a mix-solution of absolute ethanol and water using the silane coupling agent, MPS, similarly with a method in the previous work by Rong *et al.*[27] Briefly, 5 g of nano-TiO_2 was firstly dispersed in 108 mL of absolute ethanol, and into which 2.83 g of water, 1.70 g of ammonia (25 wt %), and 2.52 g of MPS were added. The mixture was firstly treated by ultrasonication and mechanically stirred at room temperature for 1 h, and then moved to an oil bath at 75 °C for further reaction for another 1 h. At last, the dispersion solution was stirred at room temperature for 22 h. The dispersion was centrifuged and redispersed in ethanol to be purified from free MPS for three cycles.

Into a three-necked round-bottom flask fitted with a condenser, 2.0 g of nano-TiO_2 particles modified by MPS coupling agent was dispersed in 80 mL DMAc. The mixture was vacuumized for 30 min and then degassed with nitrogen for another 30 min. Then, 3.0 g of HEMA and 0.3 g of initiator AIBN were added into the mixture under the atmosphere of nitrogen and followed by degassing with nitrogen for 30 min. The free radical polymerization of HEMA at the surface of nano-TiO_2 was performed at 70 °C in the nitrogen atmosphere for 12 h. Then, the modified nanoparticles (TiO_2-PHEMA) were washed thoroughly with DMAc to remove free HEMA and PHEMA or AIBN for three times, and finally washed with absolute ethanol and dried in vacuum at 60 °C for 24 h.

Characterization of TiO_2-PHEMA Nanoparticles

The characterizations of modified and unmodified particles were performed on a thermogravimetric analysis-differential scanning calorimetry (TG–DSC) instruments-STA 449F3 from NETZSCH. The samples were heated under nitrogen at a rate of 10 °C/min, from 40 °C to 700 °C and equilibrated at 40 °C for 10 min. In order to get a visual comparison between the modified and unmodified nano-TiO_2, sedimentation test was carried out. Fourier transform infrared spectroscopy (ATR-FTIR, Equinox 55, Germany) was used to characterize the formation of covalent bonds during the modification process. For further analyze of the dispersibility of modified TiO_2, the particles were observed by transmission electron microscopy (TEM, JEM-2100, Japan) in ethanol solution and a scanning electron microscope (SEM, JSM-7800F, Japan) in membrane matrix polymer.

Fabrication of PSf Membrane Substrates

The fabrication of membrane substrates were based on the classical non-solvent induced phase separation (NIPS) technique. The composition of casting solution is presented in Table I. TiO_2-PHEMA nanoparticles were added into a three-neck flask containing a certain amount of NMP and PEG-400, and stirred at room temperature to form a homogenous suspension under ultrasonic for an hour. Then PSf was added into the flask under continuous stirring. After all the materials were added, the mixture was transferred into an oil bath and stirred at 200 rpm for 24 h at 60 °C. The obtained homogenous solution was vacuumized and left at room temperature for 12 h to completely remove air bubbles. Afterward, the membrane was cast on a glass plate with a thickness of 150 μm, followed by immersion into a room temperature water coagulation bath for phase inversion process to take place. Then, the obtained membrane substrates were shook in DI water before test and interfacial polymerization (IP). These substrate membranes were hereafter coded as PSf, PSf1, PSf2, and PSf3, depending on the TiO_2-PHEMA loading in the casting dope.

Preparation of Polyamide Active Layer

The active layer of TFC FO membrane was prepared via IP process using MPD and TMC on the surface of a pre-cast PSf substrate.[28] Briefly, 2 wt % MPD aqueous solutions were poured on top of the flat sheet membrane substrates for 120 s. Then, the excess solution

Table I. Preparation Conditions of Substrates

Substrate	PSf (wt %)	PEG 400 (wt %)	NMP (wt %)	TiO_2-PHEMA (wt %)
PSf	16	6	78	0
PSf1	16	6	77	1
PSf2	16	6	76	2
PSf3	16	6	75	3

on the membrane surface was carefully removed with a filter paper. Subsequently, only the top surface of the substrate membrane was brought into contact with a 0.15 wt % TMC/*n*-hexane solution for 90 s to allow the polymerization to be performed. The resultant composite membranes were further processed at 80 °C for 8 min in an oven to achieve the desired membrane performance. Then the prepared TFC membranes were washed and stored in DI water before RO/FO measurements. These composite membranes prepared with different substrate as listed in Table I were labeled as TFC, TFC-1, TFC-2, and TFC-3, separately.

Characterizations of Membranes

Morphology, Contact Angle, and Membrane Porosity. Attenuated total reflectance Fourier transform infrared spectroscopy (ATR-FTIR, Equinox 55, Germany) was used to analyze the changes of functional groups on PSf support membrane and composite TFC membranes.

Field emission scanning electron microscopy (FESEM, JSM-7800F, Japan) was performed to examine the morphologies of the substrates and composite membranes. All membrane samples were broken in liquid nitrogen and then sputtered with gold to produce electric conductivity before examination.

To evaluate membrane surface hydrophilicity, water contact angle was measured by a contact angle meter (JC2000C Contact Angle Meter, Powereach, Shanghai, China). Before testing, the membrane samples were dried at room temperature for 48 h. At least three measurements for each membrane sample were evaluated to reduce error.

To characterize the substrate overall porosity, membranes sheets (2.5 cm × 2.5 cm) were immersed in absolute ethanol, and after 3 h ethanol-soaked substrates were taken out and carefully removed excess ethanol on the surface with tissue paper. Then the wet membranes were immediately weighed (w_1, g), dried in the oven at 50 °C for 24 h, and re-weighed (w_2, g). The membrane thickness (l, μm) was measured by a thickness gauge (Chengliang Tools Groups Co. Ltd., Chengdu, China). Then the overall porosity was calculated using eq. (1) as follows[18,29]:

$$\varepsilon = \frac{w_1 - w_2}{\rho \times A_m \times l} \tag{1}$$

where, ρ (g/cm^3) is the ethanol density, A_m (m^2) is the effective membrane area.

Mechanical Strength. The bursting strength and tensile strength of the substrates were tested to investigate the mechanical strengths. The membrane disc was placed in the infiltration cell, then increased the vertical water pressure gradually and recorded the pressure which burst the membrane and taken as bursting strength. Tensile strength was measured by XLW-500N material test-machine (Labthink, Jinan, China) at a loading velocity of 25 mm/min. The membranes were first cut into stripes with 10 mm width and an initial length of 30 mm. For each casting condition at least three stripes were tested to obtain the average values of tensile strength and extension at break.

Intrinsic Permeation Properties of TFC Membranes. A cross-flow RO filtration test cell with an effective filtration area of 15.89 cm^2 was used to evaluate the water permeability and selectivity of TFC membranes. In all RO experiments, each membrane needs to be pre-compacted under 0.8 MPa for 30 min to make sure the membrane remained in a steady state. Then the pressure was lowered to 0.6 MPa to test the performance of TFC membranes. Pure water flux (J, L/m^2 h) and water permeability (A, L/m^2 h 0.1 MPa)[30] of membranes were evaluated using the following equations.

$$J = \frac{\Delta V}{A_m \Delta t} \tag{2}$$

$$A = \frac{J}{\Delta P} \tag{3}$$

where, ΔV (L), Δt (h), and ΔP (MPa) are the permeate volume, duration, and applied pressure difference, respectively.

Salt rejection rate of membrane was measured using feed solution containing 10 m*M* NaCl solution at 0.6 MPa. To calculate membrane salt rejection rate R, the following equation was employed.

$$R = \frac{C_f - C_p}{C_f} \times 100\% \tag{4}$$

where, C_f (mol/L) and C_p are the salt concentrations in the feed and permeate solution, respectively. NaCl solution concentrations were calculated by the electrical conductivity of the salt solution which was measured by a conductivity meter (DDS-12DW, Shanghai Bante Instruments, China). The salt permeability coefficient (B, L/m^2 h),[14] which is an intrinsic property of a membrane to hold salt, is determined during RO experiment based on the solution-diffusion theory. The salt permeability coefficient is calculated by

$$\frac{1-R}{R} = \frac{B}{A(\Delta P - \Delta\pi)} \tag{5}$$

where, ΔP is the pressure difference, A is the water permeability, and $\Delta\pi$ (MPa) is the osmotic pressure difference across the membrane.

Evaluation of FO Performance. The measurement of pure water flux and reverse salt flux through the TFC FO membranes was carried out using the lab-scale filtration unit with effective membrane area of 10.0 cm^2.[31] Feed and draw solutions flowed co-currently through the channels partitioned by FO membrane at a same flow rate of 10 L/h. The FO performance was evaluated in both AL-DS mode and AL-FS mode with DI water and 2*M* NaCl were used as the feed and draw solution separately. A digital weight balance was placed at the bottom of the feed solution tank to precisely measure the water flux of the membrane. And the salt concentration changes in the feed solution were monitored with a conductivity meter. All measurements were carried out at room temperature for at least three times and the average values were reported. For each test, the averaged flux was obtained during 30 min after running for 30 min to make sure a steady state could be reached for each test.

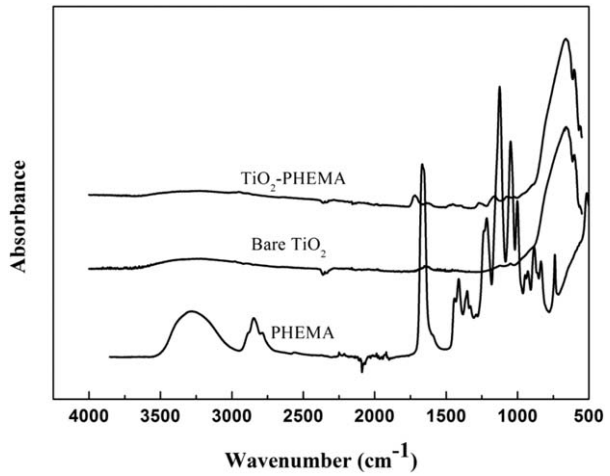

Figure 1. ATR-FTIR spectrum of TiO_2, PHEMA, and TiO_2-PHEMA.

The pure water flux, J_v (L/m^2 h) and the reverse salt flux, J_s (g/m^2 h) were calculated from eqs. (6) and (7) below:

$$J_v = \frac{\Delta V}{\Delta t A_m} \tag{6}$$

$$J_s = \frac{\Delta (C_t V_t)}{\Delta t A_m} \tag{7}$$

where, C, t, A_m, and V are salt concentration of the feed solution, the measurement time, the effective membrane area, and the volume, respectively.

In addition to J_v and J_s, the structure parameter (S, μm) is also an important property of FO membranes that needs to be evaluated. ICP depends greatly on the S value. According to the model developed by Loeb *et al.*,[32] the FO water flux can be calculated from the following equations for AL-DS and AL-FS as expressed in eqs. (8) and (9), respectively.[33]

$$J_v = \frac{D}{S}\left[\ln \frac{A\pi_{draw} - J_v + B}{A\pi_{feed} + B}\right] \tag{8}$$

$$J_v = \frac{D}{S}\left[\ln \frac{A\pi_{draw} + B}{A\pi_{feed} + J_v + B}\right] \tag{9}$$

where, D (m^2/s) is the solute diffusion coefficient; π_{draw} and π_{feed} are the osmotic pressures of the draw solution and feed solution, respectively. The membrane structural parameter S which can be represented as follows[34]:

$$S = \frac{l\tau}{\varepsilon} \tag{10}$$

where, ϵ, τ, and l are porosity, tortuosity, and thickness of the membrane, respectively.

RESULTS AND DISCUSSION

Characteristics of Modified TiO_2 Nanoparticles

Figure 1 shows the ATR-FTIR spectra of TiO_2, PHEMA, and TiO_2-PHEMA in the 500–4000 cm^{-1} region. Compared with TiO_2 and PHEMA, the spectrum of TiO_2-PHEMA showed some characteristic absorption peaks at 3411 cm^{-1}, 697 cm^{-1}, 1727 cm^{-1}, and 1161 cm^{-1} which were attributed to stretching vibrations of the –OH groups, Ti—O—Ti linkages in TiO_2 nanoparticles, stretching vibration

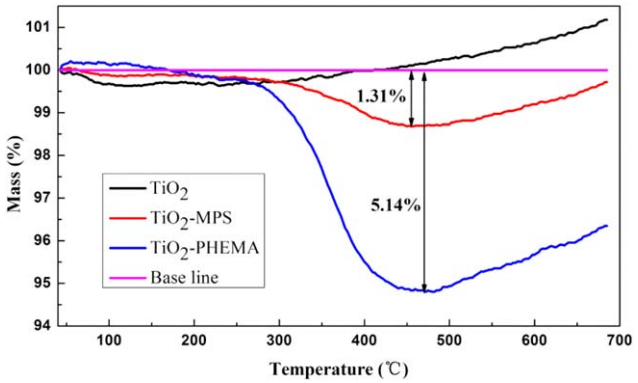

Figure 2. TGA curves of TiO_2, TiO_2-MPS, and TiO_2-PHEMA. [Color figure can be viewed in the online issue, which is available at wileyonlinelibrary.com.]

of C═O and C—O—C associated with HEMA units, respectively. Due to the linkage between TiO_2 and PHEMA, we saw a blue shift of the characteristic peaks of —C═O and C—O—C. The FTIR results confirmed the presence of HEMA chains on the nano-TiO_2 surface.

TGA was performed on both modified and unmodified nanoparticles to further characterize that HEMA chains were grafted on the TiO_2 surface and to determine the weight amount of MPS or HEMA on the nano-TiO_2 particles (Figure 2). No weight loss of pure TiO_2 was observed when heated from 40 °C to 700 °C, and a weight loss of 1.31% and 5.14% were obtained for the MPS-modified TiO_2 and HEMA-modified TiO_2, respectively, from 300 °C to 500 °C. The TGA results also proved that HEMA chains were grafted to the TiO_2 surface successfully.

Since NMP is the solvent used for membrane preparation in this study, sedimentation test in NMP for visual comparison between the unmodified nano-TiO_2 and the modified nano-TiO_2 was essential (Figure 3). Clearly, both TiO_2 and TiO_2-PHEMA could be dispersed homogenously in NMP after ultrasonication for 1h [Figure 3(A)]. After still standing for 24 h, the difference between the nano-TiO_2 and TiO_2-PHEMA [Figure 3(B)] was conspicuous

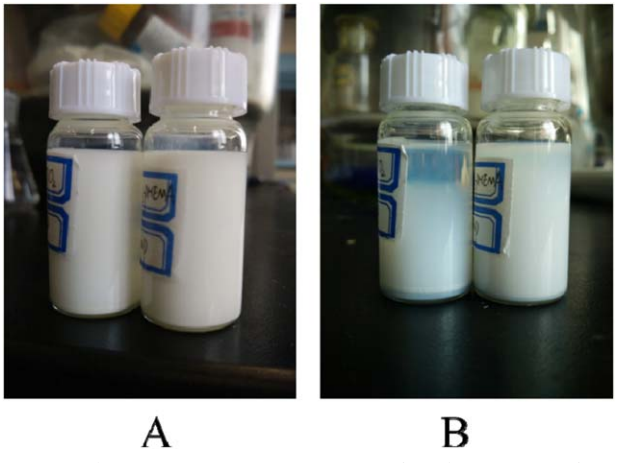

Figure 3. Sedimentation experiment in NMP after ultrasonication for 1 h (A) and still standing for 12 h (B): the left bottle is pure TiO_2 and the right one is TiO_2-PHEMA. [Color figure can be viewed in the online issue, which is available at wileyonlinelibrary.com.]

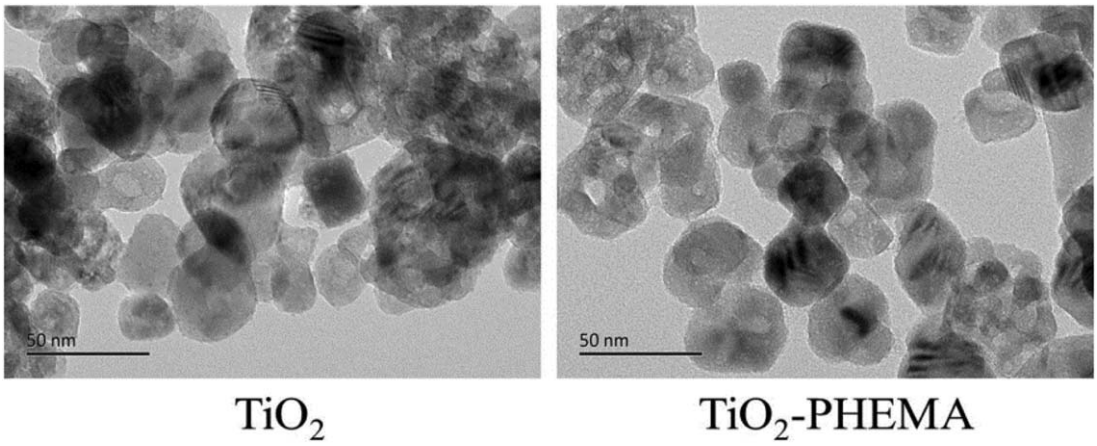

Figure 4. TEM images for TiO_2 and TiO_2-PHEMA.

Table II. Properties of Membrane Substrates

Membranes	Overall porosity (%)	Contact angle (°)	Pure water flux (L/m^2 h)[a]	BSA rejection (%)[b]
PSf	58.5 ± 1.0	77.2 ± 0.8	138.9 ± 3.8	98.7 ± 0.6
PSf1	62.5 ± 0.9	73.7 ± 1.0	280.1 ± 3.8	96.9 ± 0.8
PSf2	67.8 ± 1.6	67.8 ± 0.3	372.7 ± 13.9	95.2 ± 0.8
PSf3	60.2 ± 2.7	63.0 ± 1.8	440.6 ± 15.0	89.9 ± 0.3

[a] Pure water flux was tested in ultrafiltration mode at operating pressure of 0.1 MPa with DI water as feed solution.
[b] Bovine serum albumin (BSA) rejection rate was determined in ultrafiltration mode at 0.1 MPa with 1 g/L BSA solution as feed solution.

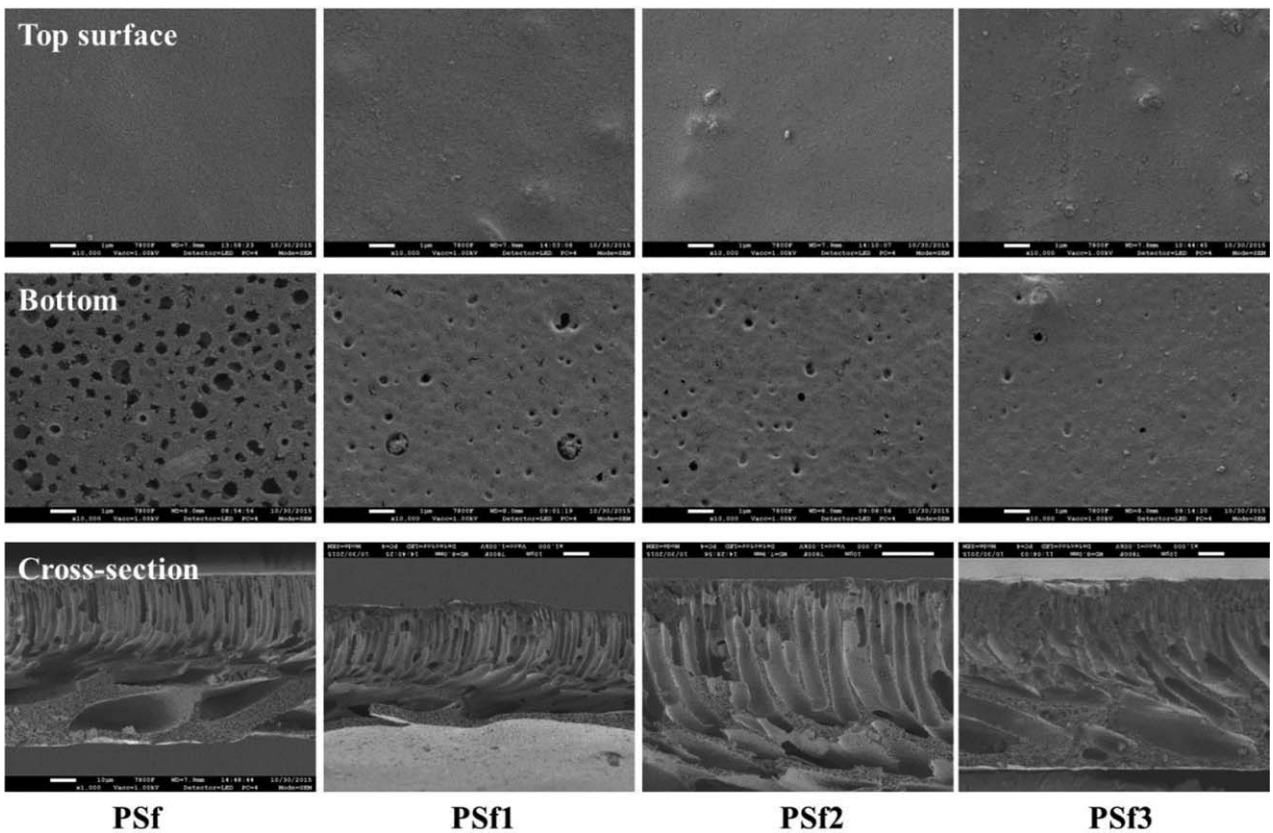

Figure 5. FESEM images of substrates with different concentrations of TiO_2-PHEMA for TFC fabrication: PSf, PSf1, PSf2, and PSf3.

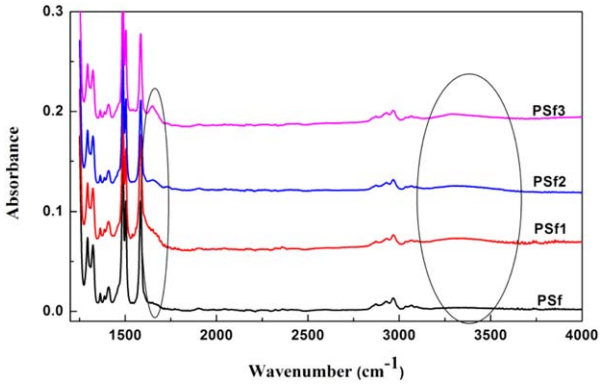

Figure 6. ATR-FTIR spectrum of substrates with different TiO_2-PHEMA loadings. [Color figure can be viewed in the online issue, which is available at wileyonlinelibrary.com.]

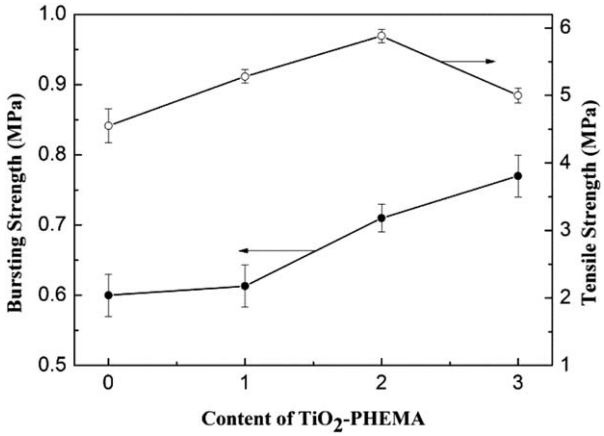

Figure 7. Mechanical strength of substrates made of different TiO_2-PHEMA loadings.

in visual comparison. Sedimentation test illustrated that unmodified nano-TiO_2 settled down more rapidly than TiO_2-PHEMA. The results obviously showed that the graft of PHEMA chains onto the surface can significantly improve the dispersibility of nano-TiO_2 in the NMP solution.

Figure 4 represents the TEM images of the unmodified nano-TiO_2 and TiO_2-PHEMA nanoparticles dispersed in ethanol. It could be seen that the unmodified TiO_2 nanoparticles aggregated seriously and it was difficult to distinguish one particle from the other. The dispersibility of TiO_2 nanoparticles was greatly improved and large area aggregates were not observed after surface modification. Therefore, the dispersibility of TiO_2 in organic solution could be significantly improved.

Properties and Performance of Membrane Substrate

Membrane properties, such as hydrophilicity, mechanical strength, morphology, and porosity could be influenced significantly by blending a hydrophilic material into the casting solution. Table II presents the changes in the substrate properties upon addition of TiO_2-PHEMA nanoparticles at different loadings. The addition of TiO_2-PHEMA promoted to form a thermodynamic unstable system, resulting in a quick phase separation and increase of porosity. However, the content of nanoparticles was further increased to 3 wt %, due to the increase of viscosity, a delayed demixing happened, and led to a sponge-like structure and decrease of porosity. By increasing the content of nanoparticles from 0 to 3 wt %, the pure water flux of substrate increased from 138.9 L/m^2 h to 440.6 L/m^2 h, recording 217% improvement, and on the contrary, led to a decrease in BSA rejection. The increase of overall porosity and membrane hydrophilicity (water contact angle decreased from 77.2° to 63.0°) were advantageous to the increase of water flux. Moreover, the decrease of BSA rejection to 89.9% for PSf-3 was mainly because of aggregation of nanoparticles at a higher concentration.

Figure 5 shows the FESEM images of the cross-section, top and bottom surfaces of PSf substrates prepared with various TiO_2-PHEMA nanoparticles loadings. The overall thickness of all the substrates fabricated with different conditions was in the range of 60–70 μm. From the SEM images, it could be clearly observed that more nanoparticle agglomeration took place on the top surface of membrane as the TiO_2-PHEMA loading increased. The cross-section of the pure PSf showed a typical

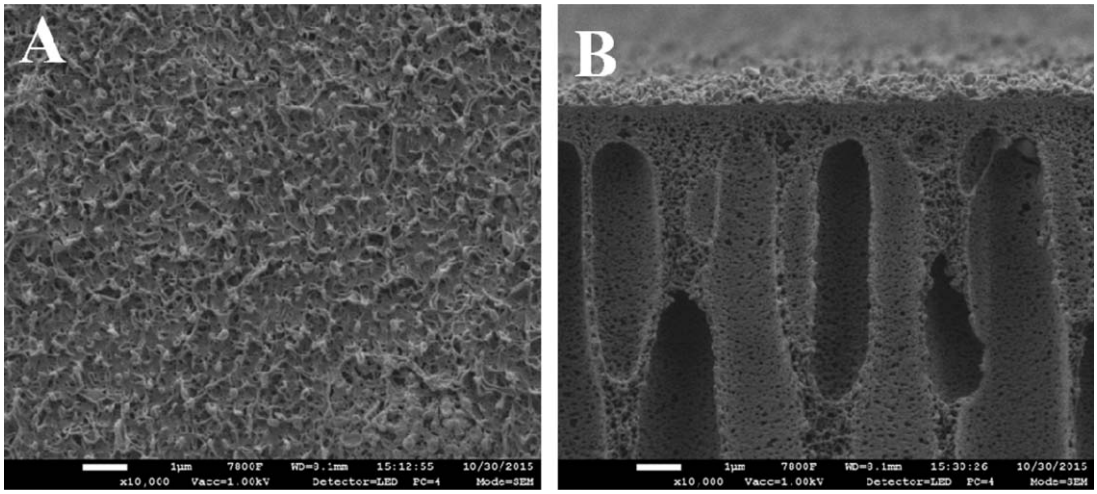

Figure 8. FESEM images of TFC-FO membrane with 2 wt % loading of TiO_2-PHEMA in the support layer.

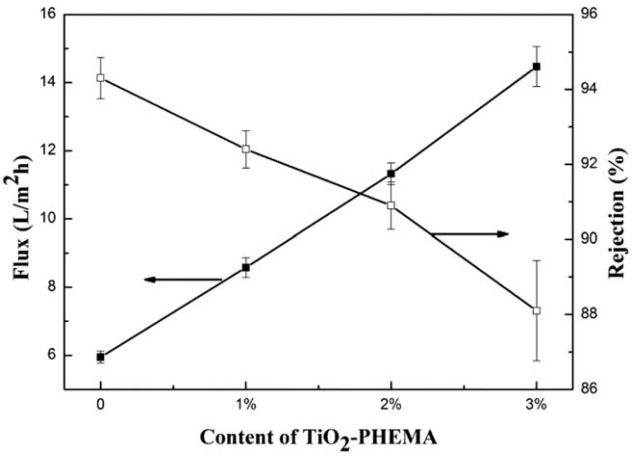

Figure 9. Water flux and salt rejection of TFC-FO membranes (test conditions: 6.0 bar, 25 °C and 10 m*M* NaCl aqueous solution as the feed).

morphology of finger-like macrovoids which was similar to those literature reports made from PSf.[35,36] On the other hand, when the content of TiO_2-PHEMA increased to 3 wt % the membrane substrate exhibited a structure consisting of sponge-like and finger-like structures. This could be explained by the delayed demixing induced by the TiO_2-PHEMA which would reduce the formation of macrovoid at higher content. Meanwhile, a lot of pores could be easily observed at the bottom surface of membranes cast from solutions comprising 0 wt % TiO_2-PHEMA, while a trace of macrovoids could be found in those membranes containing 3 wt % hydrophilic nanoparticles.

The existence of TiO_2-PHEMA in membrane substrates was further confirmed by ATR-FTIR spectrum, as shown in Figure 6. Compared to the pure PSf substrate, all the nanocomposite substrates showed absorbance peaks at around 1650–1700 cm^{-1} and 3300 cm^{-1}, which indicated the existence of C═O and –OH groups, respectively.

Figure 7 summarizes mechanical strengths of these substrates. Both bursting strength and tensile strength increased with the content of nanoparticles in the substrates. This could be explained that the addition of hydrophilic nanoparticles changed the membrane morphology and resulted in a thicker and denser skin. With a better mechanical strength, membranes can easily maintain integrity during utilization. However, when the loading of nanoparticles was increased to 3%, the tensile strength declined. This could be explained by the aggregation of TiO_2-PHEMA which led to stress concentration within the membrane.

Evaluation of TFC-FO Membrane Intrinsic Permeation Properties

Figure 8 displays the FESEM images of TFC-FO membrane on a substrate comprising 2 wt % nanoparticles and the selective polyamide layer showed a typical morphology of ridge-and-valley. From the images we can conclude that the PA layer was successfully introduced to the substrates. As shown in Figure 9, the influence of addition of the TiO_2-PHEMA on the water flux and salt rejection of those TFC films were tested. It is evident that the existence of hydrophilic nanoparticles in the substrates can greatly enhance the water permeability of TFC membranes. Pure water flux increased with the content of TiO_2-PHEMA in the substrates and reached to 14.47 L/m^2 h while 3 wt % of nanoparticles were added which was about 2.43 times of the TFC membrane (5.95 L/m^2 h). The increment of water permeability was mainly attributed to the better hydrophilicity and higher porosity of the nanocomposite substrates. From this study we could suggest that optimizing membrane substrate could provide an effective approach to enhance the permeability of the resultant TFC membranes. Figure 9 also shows the NaCl rejections of the membranes. In general, all TFC membranes possessed relatively high rejections. On the other hand, the rejection declined from 94.3% (TFC) to 88.1% (TFC-3), and this could be explained that the high TiO_2-PHEMA loading of 3 wt % in the substrate may compromise the integrity of polyamide rejection layer. This result is consistent with the FESEM observation that some localized defects were present in the PSf3 substrate. The *B*/*A* values of the various membranes are tabulated in Table III. A lower ratio of *B*/*A* is generally preferred for both RO and FO membrane processes. In the current study, both TFC-1 and TFC-2 had relatively low *B*/*A* ratios, indicating their superior separation properties.

Forward Osmosis Performance of TFC-FO Membranes

The FO water flux J_v and solute flux J_s of all TFC membranes are presented in Figure 10 for 2*M* NaCl as draw solution and DI water was used as the feed solution. As expected, greater water flux in both AL-FS and AL-DS modes were observed by increasing the content of TiO_2-PHEMA in the substrates. The TFC-3 has the highest water fluxes of 43.8 and 24.2 L/m^2 h for AL-DS and AL-FS modes, respectively, by using a 2*M* NaCl as the draw solution. However, the salt leakage were also increased

Table III. Comparison between the Permeation Properties of TFC Membranes Prepared in this Work and Commercial CTA Membranes

Membranes	Water permeability A (L/m^2 h bar)	Salt permeability B (L/m^2 h)	B/A (kPa)	References
TFC	0.99 ± 0.03	0.33 ± 0.03	33.40 ± 0.03	In this work
TFC-1	1.43 ± 0.05	0.64 ± 0.03	45.13 ± 0.03	In this work
TFC-2	1.89 ± 0.05	1.05 ± 0.10	55.39 ± 0.04	In this work
TFC-3	2.41 ± 0.10	1.80 ± 0.24	74.60 ± 0.10	In this work
HTI-CTA	0.67	0.40	59.7	37
HTI-w	0.33	0.15	45.5	38
HTI-nw	0.47	0.10	21.3	38

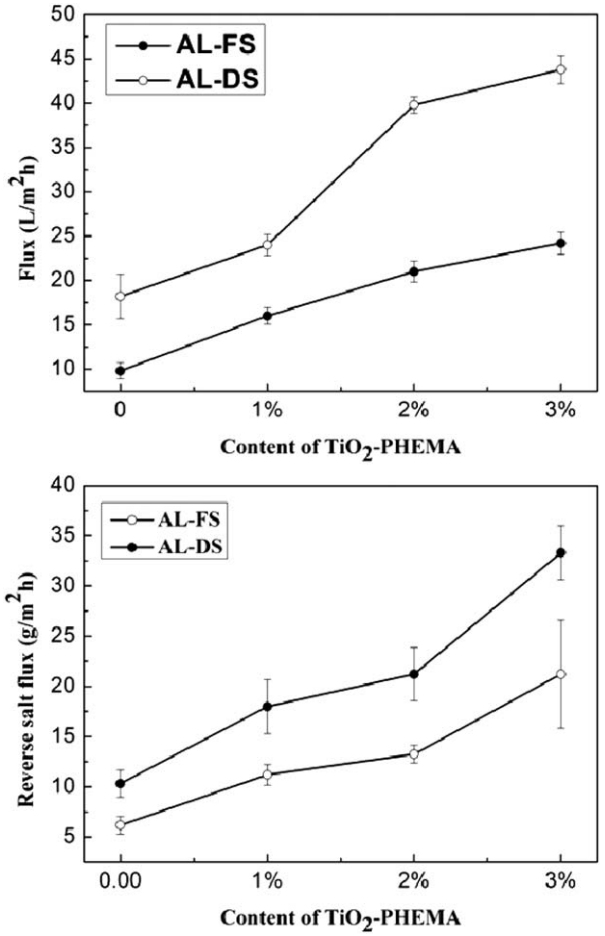

Figure 10. Pure water flux (Top) and reverse salt flux (Bottom) of TFC-FO membranes in AL-FS and AL-DS tests with 2*M* NaCl solution as draw solution and DI water as feed solution.

which was mainly due to decrease of the salt rejection. In comparison of AL-DS and AL-FS data in Figure 10, the water fluxes in the AL-DS mode for all TFC-FO membranes are much higher than those of AL-FS mode. In the AL-DS mode, the ICP was mainly caused by solute leakage, and all of the TFC membranes have relative higher rejection which would lead to less severe ICP. However, in the AL-FS mode, the water fluxes are reduced remarkably because of the severe ICP effect within the porous substrate which cannot be removed by changing operation conditions.

Generally, it is well accepted that ideal membrane support morphology should consist of a large portion of finger-like structure with a thin layer of sponge-like structure near the membrane top surface to enhance water transport through the TFC-FO membranes.[35] But in this work we get a contrary conclusion that the TFC-FO membranes with a sponge-like structure combined with finger-like structure exhibits the highest water flux in FO tests as compared to those with fully finger-like structure. It is easy to find that the porous and hydrophilic nature of our membrane substrates plays a significant role in the performance enhancement.

Table IV compares the performance and structural parameters of membranes prepared in this work with the commercial cellulose triacetate or others' work and the results are shown in Table IV. Particularly, all the TFC-FO membranes fabricated in this work have smaller structural parameters. This indicates that FO membranes fabricated on substrates with higher hydrophilic and porous nature can suffer a less severe ICP effect and achieve higher water fluxes.

CONCLUSIONS

In this work, systematic experiments were conducted to introduce the effects of different contents of hydrophilic TiO_2-PHEMA in the membrane substrates on the overall membrane morphology and FO performance. It reveals a finding that the TFC-FO membranes derived from substrates of sponge-like structures with hydrophilic nature was also able to facilitate a higher water flux in FO processes. The following conclusions can be further drawn from this work:

1. Most hydrophilic TFC membrane substrate exhibited a combined structure morphology and the highest water flux of 43.8 and 24.2 LMH tested under AL-DS and AL-FS modes, respectively, against DI water with 2*M* NaCl as the draw solution. On the contrary, the less hydrophilic membrane with a fully finger-like structure showed relative low water fluxes of 18.2 and 9.8 LMH tested under AL-DS and AL-FS modes, respectively, against DI water with 2*M* NaCl as the draw solution.

Table IV. Comparison of Performance and Structural Parameters of FO Membranes

Membranes	Water flux, LMH AL-FS/AL-DS	S[a] (μm)	Feed–draw solution	References
TFC	9.8 ± 0.9/18.2 ± 2.5	1347 ± 157	DI water–2*M* NaCl	This work
TFC-1	16 ± 0.9/24 ± 1.2	774 ± 53	DI water–2*M* NaCl	This work
TFC-2	21 ± 1.2/39.8 ± 0.9	589 ± 48	DI water–2*M* NaCl	This work
TFC-3	24.2 ± 1.2/43.8 ± 1.6	531 ± 47	DI water–2*M* NaCl	This work
HTI-nw	8.5/21.8	678	10 mM NaCl–2*M* NaCl	38
HTI-w	12.1/22.9	1000	10 mM NaCl–2*M* NaCl	38
HTI-hw	18.3/35.9	1380	10 mM NaCl–2*M* NaCl	38
TFC	14.0/33.9	782	DI water–2*M* NaCl	39
CAP-II-TFC	16.7/35.0	695	DI water–2*M* NaCl	15

[a] Structural parameters were calculated based on experiments under the FO mode using 2*M* NaCl as the draw solution and DI water as the feed [eq. (9)].

2. The structural parameter S could also be decreased remarkably with an increase in TiO_2-PHEMA content in membrane substrates.

ACKNOWLEDGMENTS

The authors sincerely appreciate the financial support from the National Key Technology R&D Program of China (No. 2014BAI11B13), National Natural Science Foundation of China (No. 21206157), and Science and Technology Foundation of Dalian (2013J21DW030).

NONMENCLATURE

C_f	Salt concentration in the feed (mol/L)
C_p	Salt concentration in the permeate volume (mol/L)
C_t	Salt concentration (mol/L)
A	Water permeability coefficient (L/m^2 h bar)
B	Solute permeability coefficient (L/m^2 h)
A_m	Effective membrane area (m^2)
D	Solute diffusion coefficient (m^2/s)
J	Water flux (L/m^2 h)
J_v	Forward osmosis water flux (L/m^2 h)
J_s	Reverse salt flux (g/m^2 h)
ρ	Solution density (g/cm^3)
P	Hydraulic pressure (MPa)
l	Membrane thickness (m)
ϵ	Membrane porosity (%)
π	Osmotic pressure (MPa)
τ	Tortuosity (dimensionless)
S	Membrane structural parameter (m)
w_1	Weight of wet membrane (g)
w_2	Weight of fry membrane (g)
V	Water permeation volume (L)
t	Operation time (h)
R	Salt rejection (%)

REFERENCES

1. Akther, N.; Sodiq, A.; Giwa, A.; Daer, S.; Arafat, H. A.; Hasan, S. W. *Chem. Eng. J.* **2015**, *281*, 502.
2. Zhou, Z. Z.; Lee, J. Y.; Chung, T. S. *Chem. Eng. J.* **2014**, *249*, 236.
3. Cath, T. Y. C.; Childress, A. E.; Elimelech, M. *J. Membr. Sci.* **2006**, *281*, 70.
4. Shannon, M. A.; Bohn, P. W.; Elimelech, M.; Georgiadis, J. G.; Marinas, B. J.; Mayes, A. M. *Nature* **2008**, *452*, 301.
5. Martinetti, C. R.; Childress, A. E.; Cath, T. Y. *J. Membr. Sci.* **2009**, *331*, 31.
6. Achilli, A.; Cath, T. Y.; Marchand, E. A.; Childress, A. E. *Desalination* **2009**, *239*, 10.
7. Cornelissen, E. R.; Harmsen, D.; De Korte, K. F.; Ruiken, C. J.; Qin, J. J.; Oo, H.; Wessels, L. P. *J. Membr. Sci.* **2008**, *319*, 158.
8. Mi, B.; Elimelech, M. *J. Membr. Sci.* **2010**, *348*, 337.
9. Ismail, A. F.; Padaki, M.; Hilal, N.; Matsuura, T.; Lau, W. J. *Desalination* **2015**, *356*, 140.
10. Klaysom, C.; Cath, T. Y.; Depuydt, T.; Vankelecom, I. F. *J. Chem. Soc. Rev.* **2013**, *42*, 6959.
11. Zhao, S. F.; Zou, L. D.; Tang, C. Y.; Mulcahy, D. *J. Membr. Sci.* **2012**, *396*, 1.
12. Widjojo, N.; Chung, T. S.; Weber, M.; Maletzko, C.; Warzelhan, V. *Chem. Eng. J.* **2013**, *220*, 15.
13. Yu, Y.; Seo, S.; Kim, I. C.; Lee, S. *J. Membr. Sci.* **2011**, *375*, 63.
14. Wang, K. Y.; Chung, T. S.; Amy, G. *AIChE J.* **2012**, *58*, 770.
15. Li, X.; Wang, K. Y.; Helmer, B.; Chung, T. S. *Ind. Eng. Chem. Res.* **2012**, *51*, 10039.
16. Park, M. J.; Phuntsho, S.; He, T.; Nisola, G. M.; Tijing, L. D.; Li, X. M.; Chen, G.; Chung, W. J.; Shon, H. K. *J. Membr. Sci.* **2015**, *493*, 496.
17. Ong, R. C.; Chung, T. S.; de Wit, J. S.; Helmer, B. J. *J. Membr. Sci.* **2015**, *473*, 63.
18. Emadzadeh, D.; Lau, W. J.; Matsuura, T.; Ismail, A. F.; Rahbari-Sisakht, M. *J. Membr. Sci.* **2014**, *449*, 74.
19. Niksefat, N.; Jahanshahi, M.; Rahimpour, A. *Desalination* **2014**, *343*, 140.
20. Goh, P. S.; Ismail, A. F. *J. Chem. Technol. Biotechnol.* **2015**, *90*, 971.
21. Mehra, N. K.; Mishra, V.; Jain, N. K. *Biomaterials* **2014**, *35*, 1267.
22. Zhang, G. L.; Lu, S. F.; Zhang, L.; Meng, Q.; Shen, C.; Zhang, J. W. *J. Membr. Sci.* **2013**, *436*, 163.
23. Emadzadeh, D.; Lau, W. J.; Rahbari-Sisakht, M.; Ilbeygi, H.; Rana, D.; Matsuura, T.; Ismail, A. F. *Chem. Eng. J.* **2015**, *281*, 243.
24. Emadzadeh, D.; Lau, W. J.; Matsuura, T.; Rahbari-Sisakht, M.; Ismail, A. F. *Chem. Eng. J.* **2014**, *237*, 70.
25. Rajaeian, B.; Rahimpour, A.; Tade, M. O.; Liu, S. M. *Desalination* **2013**, *313*, 176.
26. Zhu, L. J.; Zhu, L. P.; Jiang, J. H.; Yi, Z.; Zhao, Y. F.; Zhu, B. K.; Xu, Y. Y. *J. Membr. Sci.* **2014**, *451*, 157.
27. Rong, Y.; Chen, H. Z.; Li, H. Y.; Wang, M. *Colloids Surf. A: Physicochem. Eng. Asp.* **2005**, *253*, 193.
28. Yip, N. Y.; Tiraferri, A.; Phillip, W. A.; Schiffman, J. D.; Elimelech, M. *Environ. Sci. Technol.* **2010**, *44*, 3812.
29. Li, J. F.; Xu, Z. L.; Yang, H.; Yu, L. Y.; Liu, M. *Appl. Surf. Sci.* **2009**, *255*, 4725.
30. Rahimpour, A.; Jahanshahi, M.; Mollahosseini, A.; Rajaeian, B. *Desalination* **2012**, *285*, 31.
31. Zhang, S.; Wang, K. Y.; Chung, T. S.; Chen, H. M.; Jean, Y. C.; Amy, G. *J. Membr. Sci.* **2010**, *360*, 522.
32. Loeb, S.; Titelman, L.; Korngold, E.; Freiman, J. *J. Membr. Sci.* **1997**, *129*, 243.
33. Mehta, G. D.; Loeb, S. *J. Membr. Sci.* **1978**, *4*, 261.
34. Lobo, V. *Pure Appl. Chem.* **1993**, *65*, 2614.
35. Wang, R.; Shi, L.; Tang, C. Y.; Chou, S.; Qiu, C.; Fane, A. G. *J. Membr. Sci.* **2010**, *355*, 158.
36. Chou, S.; Shi, L.; Wang, R.; Tang, C. Y.; Qiu, C.; Fane, A. G. *Desalination* **2010**, *261*, 365.
37. Achilli, A.; Cath, T. Y.; Childress, A. E. *J. Membr. Sci.* **2009**, *343*, 42.
38. Wei, J.; Qiu, C. Q.; Tang, C. Y.; Wang, R.; Fane, A. G. *J. Membr. Sci.* **2011**, *372*, 292.
39. Ma, N.; Wei, J.; Liao, R.; Tang, C. Y. *J. Membr. Sci.* **2012**, *405–406*, 149.

SGML and CITI Use Only
DO NOT PRINT